Proceedings of the 21st ICSMGE, Vienna, Austria, 14 – 19 June 2026. Pistrol, Adam & Schweiger (eds.)
Published by: ÖGG, Austrian Society for Geomechanics, Salzburg, Austria, ISBN 978-3-9503898-4-5
https://doi.org/10.53243/ICSMGE2026-1224

Centrifuge Modeling of Silty Sand Liquefaction under Double Drainage Conditions: Validation of Scaling Laws

Mohamed E. Ghazy[1,2], Tarek Abdoun[1], Waleed El-Sekelly[1,3]
[1]New York University Abu Dhabi, United Arab Emirates; [2]Arab Academy for Science, Technology & Maritime Transport; [3]Mansoura University; m.ghazy@nyu.edu

ABSTRACT: This study investigates the effectiveness of centrifuge scaling laws under coupled dynamic and consolidation conditions through two centrifuge experiments. The experiments focused on the liquefaction behavior of silty sand under double drainage conditions, simulating a 5-m thick silty sand layer subjected to an overburden pressure equivalent to 1 atm at the mid-depth. Both tests were subjected to the same prototype base acceleration but performed at different centrifugal accelerations (20g and 45g). Key parameters such as acceleration, pore pressure generation and dissipation, and stress-strain responses were compared at various depths. The results demonstrated consistent behaviors across the studied conditions, highlighting the reliability of centrifuge modeling in capturing the dynamic behavior of silty sand under controlled drainage scenarios.

KEYWORDS: Centrifuge Modeling, Liquefaction, Silty Sand, Modeling-of-Models.

1 INTRODUCTION

Geotechnical centrifuge modeling has become a fundamental approach to studying complex soil behaviors under seismic conditions, particularly for assessing liquefaction potential. Introduced by Schofield (1981), the "modeling-of-models" technique was established as a rigorous validation strategy to evaluate centrifuge scaling laws by conducting equivalent prototype models under varying g-levels. This comparative framework offers a robust methodology to test similitude assumptions, enhancing the reliability and repeatability of centrifuge data. Over the years, it has been extensively applied in studies involving laterally loaded piles (Barton, 1985; Nunez et al., 1988; Terashi, 1989), debris flows (Bowman et al., 2010), liquefiable slopes (Zhang & Askarinejad, 2021), and internal erosion (Ovalle-Villamil & Sasanakul, 2021). Recent applications also include validating generalized scaling laws in dynamic soil-structure interaction and liquefaction-induced deformation (Korre et al., 2021; Tobita et al., 2022).

Despite the widespread application of centrifuge modeling, a key knowledge gap persists in validating the coupled scaling laws for dynamic loading and pore pressure buildup and dissipation processes, especially in low-permeability soils such as silty sands. Existing studies have either isolated the dynamic response or focused solely on fluid migration, lacking a comprehensive assessment under controlled drainage and seismic conditions. This study addresses that gap by evaluating the consistency of dynamic and consolidation behavior through two centrifuge tests at different g-levels (20g and 45g), applied to an identical silty sand prototype under double drainage conditions. Key parameters analyzed include acceleration profiles, excess pore pressure buildup and dissipation, shear stress ratio responses, and cyclic shear strains.

These two tests were conducted as part of a broader experimental campaign aimed at investigating the influence of soil permeability and silty sand stratum thickness on liquefaction resistance and the overburden correction factor K_σ , as detailed in Ghazy (2024) and Ghazy et al. (2025). Expanded findings from this campaign, including further discussion on K_σ behavior across multiple soil thicknesses, are presented in the aforementioned journal article and complementary studies. To clarify how the experimental program satisfies similitude requirements, a conceptual diagram of the coupled dynamic, consolidation, and viscous-fluid scaling laws used in this study is presented in Figure 1.

Figure 1 summarizes the combined scaling framework that underpins the modeling-of-models approach adopted in this study. Dynamic scaling ensures that the imposed cyclic stress ratio, shear strain amplitude, and acceleration input are consistent with prototype conditions. Consolidation scaling governs the time evolution of pore pressure dissipation through the nondimensional consolidation factor $T_v = c_v t/H^2$, while also maintaining the correct drainage path length at each g-level. Because silty sand exhibits relatively low permeability, viscous-fluid scaling is additionally required to match prototype hydraulic conductivity by selecting a pore fluid viscosity proportional to the applied g-level. Together, these three scaling domains establish the conditions necessary for comparable pore pressure generation, dissipation behavior, and cyclic softening across the 20g and 45g tests, thereby validating the centrifuge similitude laws employed in this investigation.

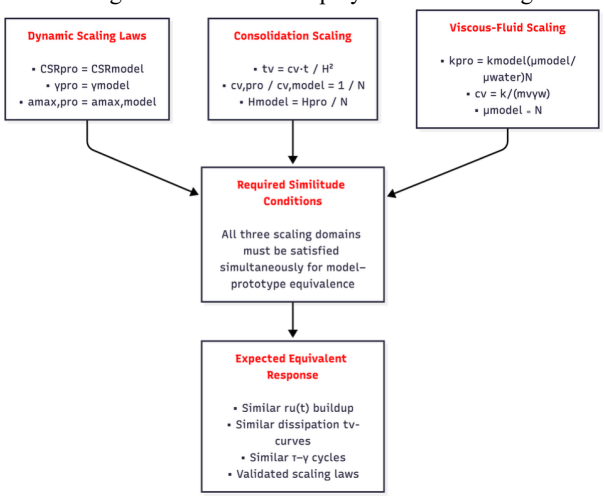

Figure 1. Conceptual diagram showing that dynamic, consolidation, and viscous-fluid scaling laws that was satisfied simultaneously.

2 EXPERIMENTAL SETUP

The experimental program simulated a 5-meter-thick silty sand layer subjected to a 1 atm overburden pressure at mid-depth, using centrifugal accelerations of 20g and 45g to create two identical prototype scenarios. The model configuration comprised three distinct layers: a liquefiable silty sand base layer, an intermediate transition coarse sand filter, and a top layer of heavy dry lead shot (Figure 2). The lead shot layer, with a high unit weight, was placed to reproduce the desired vertical effective stress (1 atm) at the middle of the silty sand stratum.

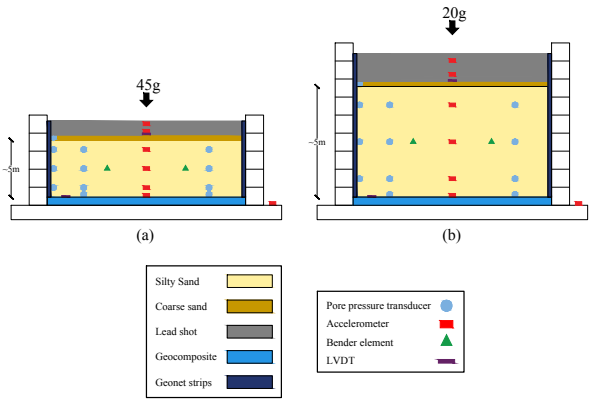

Figure 2. Experimental Setup for a) Model B-45g; b) Model A-20g

The silty sand was prepared by mixing 85% Ottawa F65 sand and 15% Sil-Co-Sil silt by weight. The soil was dry pluviated into a 1D laminar box to achieve a target relative density of approximately 45%. Saturation of the silty sand layer was performed using a viscous fluid, with viscosity tailored to each g-level—20 cp for the 20g test and 45 cp for the 45g test—ensuring field-prototype hydraulic conductivity similarity.

The tests simulated a silty sand stratum under double drainage conditions. Drainage from the top was provided through the coarse sand filter, while drainage from the bottom was facilitated using a geocomposite drainage layer connected to lateral geonet strips, allowing viscous fluid to exit the system effectively. This drainage setup was designed to match the configuration adopted by Ni et al. (2021), where more detailed descriptions of the system can be found.

Once the silty sand layer was saturated, a coarse sand transition layer was gently placed above it to act as a filter and prevent intrusion of the upper layer. Subsequently, a dry lead shot layer was carefully added to apply the overburden pressure.

Instrumentation included accelerometers at multiple depths to capture seismic response, pore pressure transducers (PPTs) to record excess pore pressure, LVDTs for vertical displacement, and bender elements for in-situ shear wave velocity. These sensors were strategically distributed in three main layers: the top, middle, and bottom of the silty sand stratum, to monitor the response across the entire depth profile. This configuration ensured a detailed resolution of the dynamic and hydraulic behavior of the soil throughout the tests.

Key details of the test conditions, including relative density (D_r), peak ground acceleration (PGA), shear wave velocity (V_s), and maximum excess pore pressure ratio (max. r_u) for both centrifuge tests, are summarized in Table 1.

Table 1. D_r, PGA, V_s and max. r_u, for centrifuge tests

Test	D_r (%)	PGA at base (g)	Shear Wave Velocity (m/sec)	$(r_u)_{max}$		
				Bottom	Middle	Top
Model A-20g	44.8	0.069	115	0.17	0.42	0.76
Model B-45g	42.3	0.064	116	0.19	0.41	0.67

3 DISCUSSION OF RESULTS

3.1 *Acceleration*

Both centrifuge models were subjected to the same base input motion using the hydraulic biaxial 2D shaker system at the Rensselaer Polytechnic Institute (RPI) centrifuge facility. The input motion consisted of a 2 Hz sinusoidal wave with a consistent amplitude tailored to generate excess pore pressure conditions approaching liquefaction in the silty sand layer, with a target maximum excess pore pressure ratio (r_u) of approximately 0.8. This level was selected to replicate behavior near the onset of liquefaction while avoiding the unpredictable and unstable responses typically observed at $r_u = 1.0$.

Figure 3 illustrates the acceleration time histories recorded at multiple depths within both models. The results show consistent amplification near the top of the silty sand layer, followed by a gradual attenuation of acceleration amplitudes with depth and with increasing excess pore pressure. This attenuation pattern reflects the softening of the soil matrix and the associated reduction in shear stiffness as pore pressure builds up during shaking. Furthermore, a comparison of acceleration responses between the 20g and 45g tests reveals strong agreement in waveform shape and amplitude distribution, confirming the effectiveness of the modeling-of-models technique. The excess pore pressure response is examined next to evaluate both buildup during shaking and dissipation afterward.

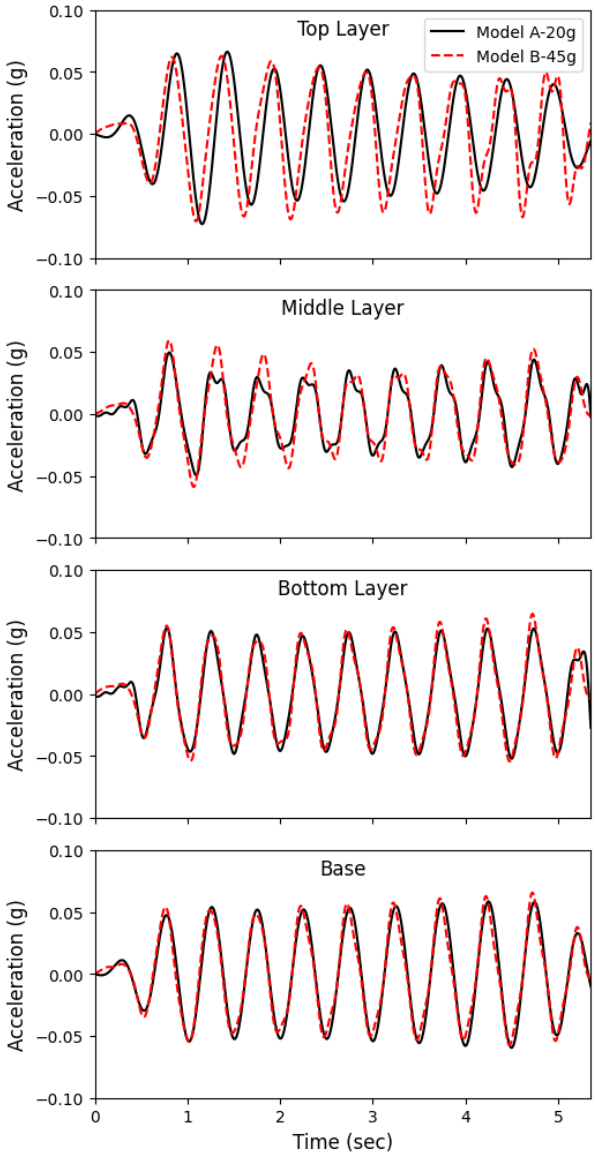

Figure 3. Acceleration time histories for Model A-20g & Model B-45g (Source: Ghazy et al. (2024))

3.2 *Excess Pore Pressure Ratio* (r_u)

Excess pore pressure ratio (r_u) , defined as the excess pore pressure (Δu) divided by the initial vertical effective stress (σ'_v), was used to assess the seismic response of the silty sand layer at each depth of the profile. The excess pore pressure was measured using pore pressure transducers (PPTs) embedded throughout the silty sand profile. To enable direct comparison of pore-pressure generation between the 20g and 45g tests, the excess pore-pressure ratio was plotted against a normalized cycle number N^*, defined as $N^* = t \cdot f$, where $t$is the prototype time and $f = 2$Hz is the input shaking frequency. Because one full loading cycle corresponds to one second of prototype time at 2 Hz, this transformation places both tests on a common, dimensionless cycle axis and removes any differences associated with g-level scaling of the time domain.

Figure 4 shows the buildup of the excess pore-pressure ratio plotted against the normalized cycle number at the top, middle, and bottom of the silty sand layer. When viewed in this dimensionless form, both centrifuge tests exhibit highly consistent pore-pressure generation behavior, with the 20g and 45g curves closely overlapping across all depths. The maximum values extracted from each test are also included in the figure, further illustrating the close agreement between the two models, and also can be shown in Table 1. A slightly higher peak value is observed at the top of the layer for the Model A-20g test; however, this difference is attributed to the pore-pressure transducer being positioned marginally closer to the drainage boundary in that model. Aside from this minor placement-related variation, the two tests show nearly identical rates of $r_u$buildup and comparable peak responses, confirming that dynamic similitude was effectively achieved at both g-levels.

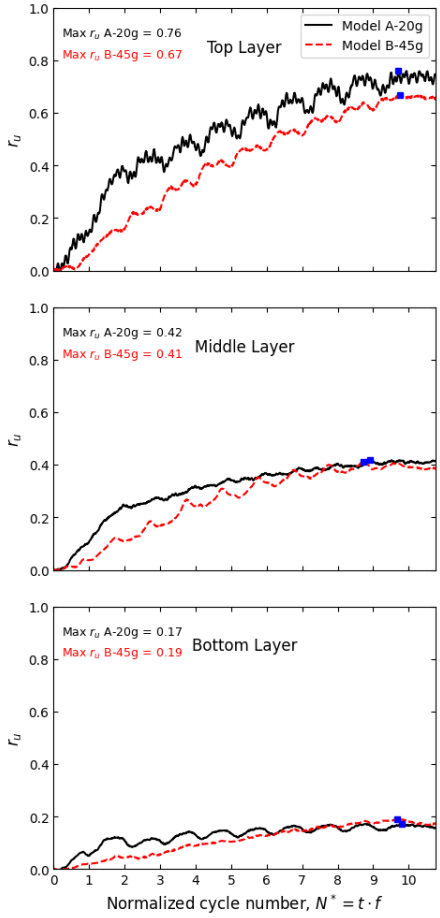

Figure 4. Normalized-cycle pore-pressure generation

Figure 5 presents the excess pore-pressure dissipation starting from the end of shaking, expressed in prototype time for both the 20g and 45g tests. Post-shaking, the dissipation of was clearly observed, influenced by the double drainage boundary conditions and the inherent permeability of the silty sand. Dissipation occurred more rapidly near the top and bottom boundaries due to the shorter drainage paths to the free-draining layers, whereas the middle portion of the layer displayed a slower rate of pore pressure dissipation. This behavior underscores the importance of drainage path length and boundary configuration in governing excess pore pressure decay during liquefaction.

Across all three depths, the dissipation curves from the two models collapse closely onto one another, indicating that both tests experienced comparable hydraulic response and permeability-controlled flow during reconsolidation. This agreement confirms that the consolidation similitude conditions and the viscosity-matching procedure successfully preserved the prototype dissipation behavior at different centrifuge accelerations.

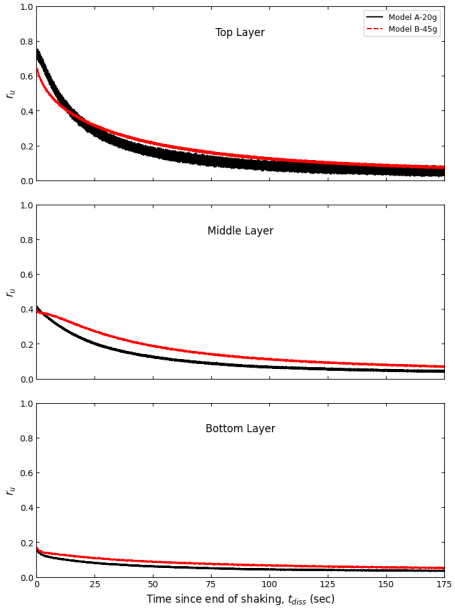

Figure 5. Pore-pressure dissipation curves beginning at the end of shaking

3.3 *Shear Stress Ratio & Shear Strain*

The shear stresses and shear strains used to construct the τ–γ hysteresis loops were computed using the system-identification (SI) method developed by Elgamal et al. (1995) and Zeghal et al. (1995) , which treats the centrifuge soil column as a vertically discretized shear beam. Horizontal acceleration records from the embedded accelerometer arrays were double-integrated to obtain relative displacements, and shear strains were then obtained by differentiating these displacement profiles over the vertical spacing of the sensors. Shear stresses were simultaneously estimated from the depth-dependent inertial forces derived from the same acceleration measurements, yielding synchronized τ–γ time histories for both centrifuge models.

Figure 6 presents the complete shear stress–strain hysteresis loops at the Middle of the silty sand layer for the 20g and 45g tests over the full shaking duration. The two models exhibit reasonably similar overall loop shapes, stress amplitudes, and strain ranges, demonstrating that the cyclic stiffness and nonlinear stress–strain behavior were reproduced consistently across g-levels. Both tests display progressive loop

widening with continued shaking, reflecting stiffness degradation and increased material nonlinearity as pore pressure accumulates. The relatively close alignment of these full-cycle hysteresis patterns provides additional confirmation that dynamic similitude was effectively achieved and that the SI-derived stress–strain estimates remain robust across different centrifugal accelerations.

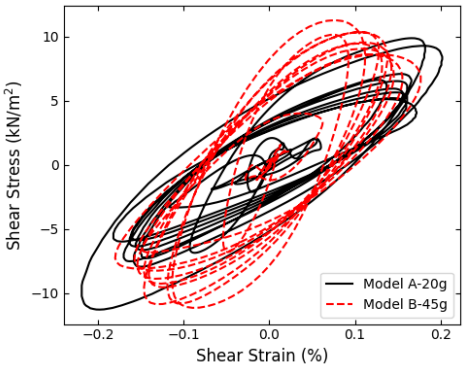

Figure 6. Shear stress–strain hysteresis loops for the 20g and 45g centrifuge tests.

4 CONCLUSION

The conducted centrifuge tests demonstrated the reliability and repeatability of seismic response characteristics of silty sand under varying gravitational conditions. Consistent acceleration amplification and attenuation, clear excess pore pressure generation and dissipation profiles, and reproducible shear stress and strain responses validate the employed experimental methodologies. The normalized-cycle pore-pressure analysis further confirmed that both g-levels produced nearly identical excess pore-pressure buildup patterns across depths, indicating strong dynamic similitude between the two tests. Post-shaking, the dissipation curves initiated at the end of shaking exhibited close agreement between the two models, reaffirming that consolidation similitude and viscosity matching collectively preserved prototype hydraulic behavior under double drainage conditions.

The findings confirm the applicability and precision of the "modeling-of-models" approach in validating centrifuge scaling laws, underscoring its significance for future seismic evaluations and soil liquefaction studies. Importantly, the study highlights the effectiveness of the viscosity-matching approach to replicate prototype hydraulic conductivity at different g-levels, allowing the same prototype response to be reproduced across multiple tests. The use of double drainage conditions enabled the investigation of realistic field scenarios where dissipation occurs through both the top and bottom boundaries. Notably, the observed trends in pore pressure dissipation—faster at the boundaries and slower at mid-depth—emphasize the relevance of drainage path length and boundary conditions on excess pore pressure evolution.

Furthermore, the full-cycle shear stress–strain hysteresis loops demonstrated agreement in cyclic stiffness, nonlinearity, and stress amplitude between the 20g and 45g tests, particularly at the middle of the silty sand layer. The overall loop geometry and degradation behavior remained comparable. These results reinforce the dynamic similitude between the two tests and further validate the reliability of the system-identification method in recovering soil stress–strain behavior under centrifuge loading. Collectively, these findings support the applicability of the experimental configuration for studying seismic response in low-permeability soils and provide a comprehensive dataset for validation of advanced constitutive and numerical models.

5 REFERENCES

Barton, Y. (1985). Response of pile groups to lateral loading in the centrifuge. *Publication of: Balkema (AA)*.

Bowman, E. T., Laue, J., Imre, B., & Springman, S. M. (2010). Experimental modelling of debris flow behaviour using a geotechnical centrifuge. *Canadian Geotechnical Journal*, *47*(7), 742-762. https://doi.org/10.1139/t09-141

Elgamal, A. W., Zeghal, M., Tang, H. T., & Stepp, J. C. (1995). Lotung Downhole Array. I: Evaluation of Site Dynamic Properties. *Journal of Geotechnical Engineering*, *121*(4), 350-362. https://doi.org/10.1061/(asce)0733-9410(1995)121:4(350)

Ghazy, M. E. (2024). *Liquefaction Behavior of Silty Sand: The Influence of Permeability and Soil Thickness on Overburden Pressure Correction Factor (Kσ) Using Centrifuge Testing* (Publication Number 31556655) [Ph.D., New York University Tandon School of Engineering]. ProQuest Dissertations & Theses Global. United States -- New York. http://proxy.library.nyu.edu/login?qurl=https%3A%2F%2Fwww.proquest.com%2Fdissertations-theses%2Fliquefaction-behavior-silty-sand-influence%2Fdocview%2F3116172429%2Fse-2%3Faccountid%3D12768

Ghazy, M. E., Abdoun, T., Dobry, R., & El-Sekelly, W. (2024). Centrifuge modeling-of-models investigation on earthquake-induced excess pore pressure behavior of silty sand. *Soil Dynamics and Earthquake Engineering*, *185*. https://doi.org/10.1016/j.soildyn.2024.108906

Ghazy, M. E., Abdoun, T., Dobry, R., & El-Sekelly, W. (2025). Evaluating the Influence of Soil Stratum Thickness on Liquefaction Potential and Overburden Correction Factor Kσ in Silty Sand: A Centrifuge Study. *Journal of Geotechnical and Geoenvironmental Engineering*, *151*(9). https://doi.org/10.1061/jggefk.gteng-13480

Korre, E., Abdoun, T., Zeghal, M., & Kokkali, P. (2021). Verification of generalized scaling laws: Two centrifuge tests of a liquefiable sloping deposit. *Soil Dynamics and Earthquake Engineering*, *141*, 106480. https://doi.org/10.1016/j.soildyn.2020.106480

Ni, M., Abdoun, T., Dobry, R., & El-Sekelly, W. (2021). Effect of Field Drainage on Seismic Pore Pressure Buildup and Kσ under High Overburden Pressure. *Journal of Geotechnical and Geoenvironmental Engineering*, *147*(9). https://doi.org/10.1061/(ASCE)GT.1943-5606.0002536

Nunez, I., Phillips, R., Randolph, M., & Wesselink, B. (1988). Modelling laterally loaded piles in calcareous sand. Proc. Int. Conf. Centrifuge,

Ovalle-Villamil, W., & Sasanakul, I. (2021). Assessment of centrifuge modelling of internal erosion induced by upward flow conditions. *International Journal of Physical Modelling in Geotechnics*, *21*(5), 251-267. https://doi.org/10.1680/jphmg.20.00004

Schofield, A. N. (1981). *Dynamic and Earthquake Geotechnical Centrifuge Modelling* 1st International Conference on Recent Advances in Geotechnical Earthquake Engineering and Soil Dynamics, https://scholarsmine.mst.edu/icrageesd/01icrageesd/session05/2

Terashi, M. (1989). Centrifuge modeling of a laterally loaded pile. Proc. of the 12th International Conference on Soil Mechanics and Foundation Engineering, 1989,

Tobita, T., Ueda, K., Vargas, R. R., Ichii, K., Okamura, M., Sjafruddin, A. N., Takemura, J., Hang, L., Uzuoka, R., Iai, S., Boksmati, J., Fusco, A., Torres-Garcia, S., Haigh, S., Madabhushi, G., Manzari, M., Escoffier, S., Li, Z., Kim, D. S.,…Ma, Q. (2022). LEAP-ASIA-2019: Validation of centrifuge experiments and the generalized scaling law on liquefaction-induced lateral spreading. Soil Dynamics and Earthquake Engineering, 157, 107237. https://doi.org/10.1016/j.soildyn.2022.107237

Zeghal, M., Elgamal, A.-W., Tang, H. T., & Stepp, J. C. (1995). Lotung Downhole Array. II: Evaluation of Soil Nonlinear Properties. Journal of Geotechnical Engineering, 121(4). https://doi.org/10.1061/(ASCE)0733-9410(1995)121:4(363)

Zhang, W., & Askarinejad, A. (2021). Centrifuge modelling of static liquefaction in submarine slopes: scaling law dilemma. Canadian Geotechnical Journal, 58(2), 200-209. https://doi.org/10.1139/cgj-2019-0417